A novel approach to the functional classification of retinal ganglion cells

Short title: DREADD for RGC classification

Gerrit Hilgen[1, 2 *], Evgenia Kartsaki[1, 3], Viktoriia Kartysh[1,4,5], Bruno Cessac[3], Evelyne Sernagor[1*]

[1] *Biosciences Institute, Newcastle University, Newcastle upon Tyne, UK*

[2] *Health & Life Sciences, Applied Sciences, Northumbria University, Newcastle upon Tyne UK*

[3] *Université Côte d'Azur, Inria, Biovision team and Neuromod Institute, Sophia Antipolis Cedex, France*

[4] *Ludwig Boltzmann Institute for Rare and Undiagnosed Diseases (LBI-RUD), 1090 Vienna, Austria*

[5] *Research Centre for Molecular Medicine (CeMM) of the Austrian Academy of Sciences, 1090 Vienna, Austria*

** Corresponding author*

Email: gerrit.hilgen@northumbria.ac.uk

evelyne.sernagor@ncl.ac.uk

Abstract

Retinal neurons come in remarkable diversity based on structure, function and genetic identity. Classifying these cells is a challenging task, requiring multimodal methodology. Here, we introduce a novel approach for retinal ganglion cell (RGC) classification, based on pharmacogenetics combined with immunohistochemistry and large-scale retinal electrophysiology. Our novel strategy allows grouping of cells sharing gene expression and understanding how these cell classes respond to basic and complex visual scenes. Our approach consists of increasing the firing level of RGCs co-expressing a certain gene (*Scnn1a* or *Grik4*) using excitatory DREADDs (Designer Receptors Exclusively Activated by Designer Drugs) and then correlate the location of these cells with *post hoc* immunostaining, to unequivocally characterize anatomical and functional features of these two groups. We grouped these isolated RGC responses into multiple clusters based on the similarity of the spike trains. With our approach, and accompanied by immunohistochemistry, we were able to extend the pre-existing list of Grik4 expressing RGC types to a total of 8 RGC types and, for the first time, we provide a phenotypical description of 14 Scnn1a-expressing RGCs. The insights and methods gained here can guide RGC classification but also neuronal classification challenges in other brain regions.

Introduction

Visual processing starts in the retina, at synapses between photoreceptors and second order neurons. The retina contains two types of photoreceptors, rods for lowlight and cones for daylight and color vision. In line with rods and cones, the retina also contains rod- and cone-contacting bipolar cells. Furthermore, cone-contacting bipolar cells can be divided into ON and OFF bipolar cells and further subdivided into more than a dozen of different subpopulations [1]. These parallel processed channels are further divided into a variety of functional output channels, so-called retinal ganglion cells (RGCs), which encode different features of the visual environment. There are ~1 million RGCs in humans and ~45,000 in mice [2,3], integrating the visual information processed from photoreceptors down the retinal neural network. That integrated information is sent by RGCs as spike train codes along the optic nerve to visual brain areas [4]. Different types of RGCs extract very specific features from the visual scenery [5]. Given the remarkable diversity of functional RGC classes, each type encodes a distinct, highly compressed spike code. This code is transmitted to postsynaptic targets in the brain, leading to visual perception. At present, more than 30 RGC types have been identified in the mouse retina [6], and between 15-20 types in the primate and human retina, respectively [7,8]. RGC classification is typically based on common anatomical features [9,10], responses to light [6,11–13] or on shared gene expression [4,14,15]. Classification based on gene expression is relatively recent, and the majority of RGC groups sharing specific genes have not been phenotyped yet. Each of these RGC subpopulations exhibits a distinct spatial mosaic pattern across the retina, suggesting that these cells belong to a well-defined functional group.

Current approaches to characterize pan retinal RGC subpopulations functionally are limited. Classical recording approaches, such as patch-clamping have high temporal precision, yet low cell numbers result in poor yield. Optical methods (e.g., calcium imaging) improve the yield, but at the cost of temporal resolution which becomes too low to yield reliable spike timing, an important feature in retinal spike coding [16,17]. Moreover, imaging approaches performed at cellular resolution cannot be implemented at pan retinal level. Multielectrode arrays (MEAs), on the other hand, allow electrical recording from many RGCs simultaneously at high spatiotemporal resolution [18]. Here we use a CMOS (complementary metal-oxide-semiconductor) MEA system consisting of 4,096 electrodes (2.67 x 2.67 mm), allowing us to record light responses from hundreds to thousands of RGCs simultaneously at pan-retinal level and near cellular resolution [17,19]. We selected two genes based on their sparse distribution across the RGC layer and their novelty for phenotypic characterization (Allen Mouse Brain Connectivity Atlas (2011)). *Grik4* (glutamate receptor, ionotropic, kainite subunit 4, HGNC: 4582) expressing RGCs have only been partially described. Using a *Grik4* Cre mouse line [20], these cells are known to have a bistratified dendritic arbor [21] and are characterized functionally as ON-OFF direction selective (DS) RGCs [22,23]. *Grik4* expression is also present in ON DS RGCs [4] and in the well described Pix-ON RGC [24]. The other gene we investigated is *Scnn1a* (non-voltage gated sodium channel, epithelial 1 subunit alpha, HGNC:10599). Scnn1a Cre-induced recombination is present in sparse Layer 4 neurons, mostly in the somatosensory cortex [25] the *Scnn1a*-Tg3-Cre line [25]. Current knowledge of Scnn1a expressing RGCs in the retina is limited to their dendritic arbor stratifies in sublaminas S1 and S2 (OFF layers) and in sublamina S4 (ON layer) in the inner plexiform layer [4]. Here, we crossbred Grik4 and Scnn1a cre mice with DREADD flox mice to further investigate these RGC types.

Designer Receptors Exclusively Activated by Designer Drugs (DREADDs) [26] technology is a powerful new approach to pharmacologically dissect out the role of specific neuronal cell classes in network activity [27,28]. DREADDs are an engineered version of G-proteins that allow precise control of G-protein signaling pathways and can be activated with clozapine-N-oxide (CNO), a “designer drug” with no endogenous receptors in the organism. DREADDs are designed upon metabotropic cholinergic muscarinic receptors. Most commonly used DREADDs are excitatory (hM3Dq, triggering release of calcium from organelles leading to increase of intracellular concentration of free calcium and to membrane depolarization), or inhibitory (hM4Di, opening of potassium channels, leading to membrane hyperpolarization). In this study, we have generated Cre recombinase-mediated restricted expression of cell-specific DREADD [29] expressions in either Grik4 or Scnn1a reporter lines. We have successfully isolated light-evoked responses in RGCs sharing Scnn1a and Grik4 gene expression by combining excitatory DREADD activation, large-scale retinal CMOS MEA recording and post hoc labeling of DREADD RGCs. We grouped the RGC responses into multiple clusters based on the similarity of the spike trains they generate during a series of stationary stimuli, thus extending and unravelling RGC types for the Scnn1a and Grik4 gene pool.

Results

In order to functionally validate RGC subgroups according to shared gene expression, we first established an immunohistochemical atlas of these cells. Building such a resource for Grik4 and Scnn1a expressing cells in the mouse retina is important for estimation of the RGC numbers and types in these two genetic pools. We used the intrinsic fluorescence signal of Grik4-DREADD (hereafter named Grik4) and Scnn1a-DREADD (hereafter named Scnn1a) cells to provide a detailed IHC map of Grik4 and Scnn1a expressing cells in retinal whole mounts and vertical sections. Each DREADD is tagged with

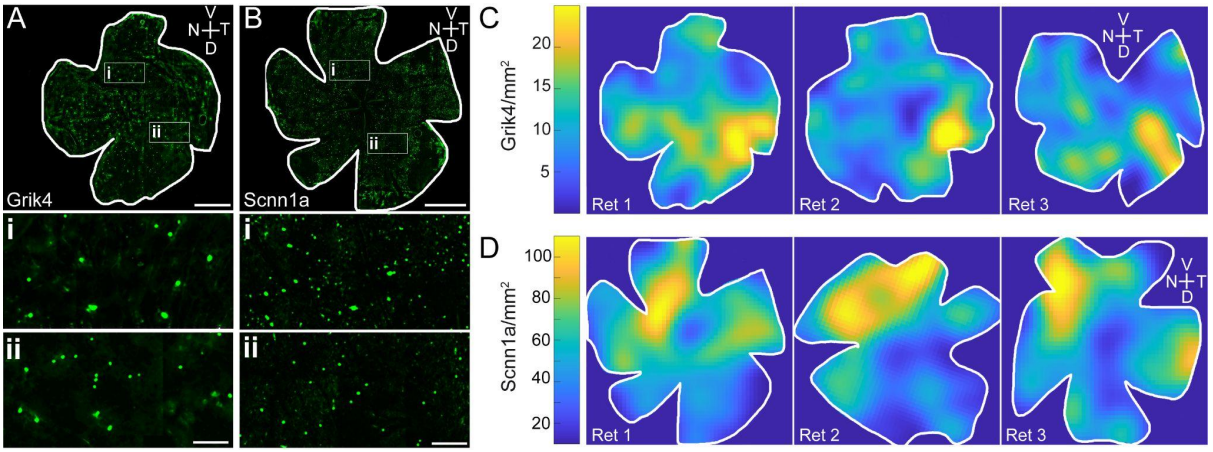

Figure 1: Grik4 and Scnn1a cells in the GCL are not spatially homogeneous distributed. Whole mount antibody staining against Grik4 (A) and Scnn1a (B) DREADD GFP were imaged at the level of the ganglion cell layer. All stained GFP cells were counted and the densities per mm^2 were calculated and presented in pseudocolors for 3 Grik4 (C) and Scnn1a (D) retinas.V= ventral, T = temporal, D = dorsal, N = nasal. Scale bar A, B = 1 mm; Scale bar A, B insets II = 100 µm.

hemagglutinin (HA) as well as mCitrine, allowing to visualize DREADD-expressing cells by immunofluorescence. We first investigated the distribution of Grik4 and Scnn1a cells in the ganglion cell layer (GCL) in retinal whole mounts using an antibody against Green Fluorescent Protein (GFP) to amplify the intrinsic mCitrine signal (Fig 1). Both lines exhibit sparse cellular distribution in the GCL, with Scnn1a cells significantly more abundant than Grik4 (Fig 1 A, B insets I and II). We calculated the cell densities in the GCL of three representative Grik4 (Fig 1 C) and Scnn1a (Fig 1 D) retinas. Grik4 and Scnn1a cell densities respectively vary between 10-25 and 40-100 cells/mm^2. Both pools exhibit non-even distributions. Grik4 cells are more prominent in the dorsal-temporal periphery (Fig 1 C, yellow areas), while Scnn1a cells are more prominent in the ventral-nasal periphery (Fig 1 D, yellow areas).

The GCL consists mainly of RGCs but it also contains displaced amacrine cells (dACs) and glial cells. We investigated whether dACs contribute to the pool of Grik4 and Scnn1a cells in the GCL. We used known specific RGC and amacrine cell (AC) markers to estimate the contribution of different RGC types in both gene pools. First, we double-labelled Grik4 and Scnn1a retinal vertical sections against GFP (Fig 2 A, B cyan) and RBPMS (Fig 2 A, B magenta), a selective marker for RGCs in the mammalian retina [30]. More than 50% of the GFP labelled Grik4 cells in the GCL are RBPMS positive (Fig 2 A, arrows) whereas the other cells are likely dACs. In support, the somata of putative dACs in the GCL are relatively small, which is a key feature of these cells. A similar pattern was found for Scnn1a cells in the GCL but here, the majority of Scnn1a cells are RGCs (Fig 2 B, arrows). Sparsely distributed cells with either Grik4 (Fig 2 C, cyan) or Scnn1a (Fig 2 D, cyan) expressions were present in the proximal inner nuclear layer (INL). These cells did not stain for RBPMS (Fig 2 A, B) and are amacrine cells (ACs). Most AC types are GABAergic, hence we initially stained

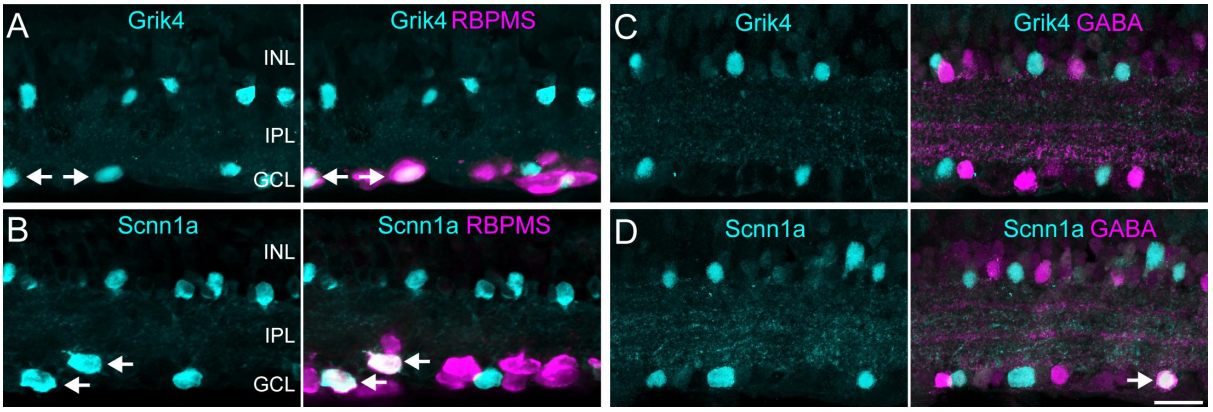

Figure 2: Grik 4 and Scnn1a DREADD are expressed in RGCs and ACs. Vertical sections were stained for Grik 4 (A, C, cyan) and Scnn1a (B, D, cyan) GFP. Sections were further co-labelled with RBPMS (A, B, magenta), a marker for retinal ganglion cells, and GABA (C, D, magenta). INL = inner nuclear layer, IPL = inner plexiform layer, GCL = ganglion cell layer. Scale bar in D = 20 µm.

GABA (Fig 2 C, D, magenta) and GFP in Grik4 and Scnn1a vertical sections. Interestingly, we could not find any GABA-positive Grik4 ACs (Fig 2 C). On the other hand, we occasionally found GABAergic Scnn1a cells in the INL or GCL (Fig 2 D, arrow). In conclusion, a major proportion of Grik4 and Scnn1a cells in the GCL are RGCs but both genes are also sparsely expressed in ACs in the INL and dACs in the GCL. Further, Grik4 cells are not GABAergic while a very small population of Scnn1a is.

To further characterize the expression patterns of Scnn1a and Grik4 in RGCs and ACs, retinal sections were stained for GFP, RBPMS and for the well-described calcium-binding protein markers Parvalbumin and Calretinin (Fig 3) [31,32]. Briefly, Parvalbumin is found in amacrine cells and in 8-14 different RGC types . Calretinin is present in amacrine cells too and can be found in 10 RGC types. In a first set of experiments (Fig 3 A, B) we labelled respectively against GFP (cyan), RBPMS (magenta) and Calretinin (yellow) in vertical sections of Grik4 (Fig 3 A) and Scnn1a (Fig 3 B) retinas. For both retinas, we found a subset

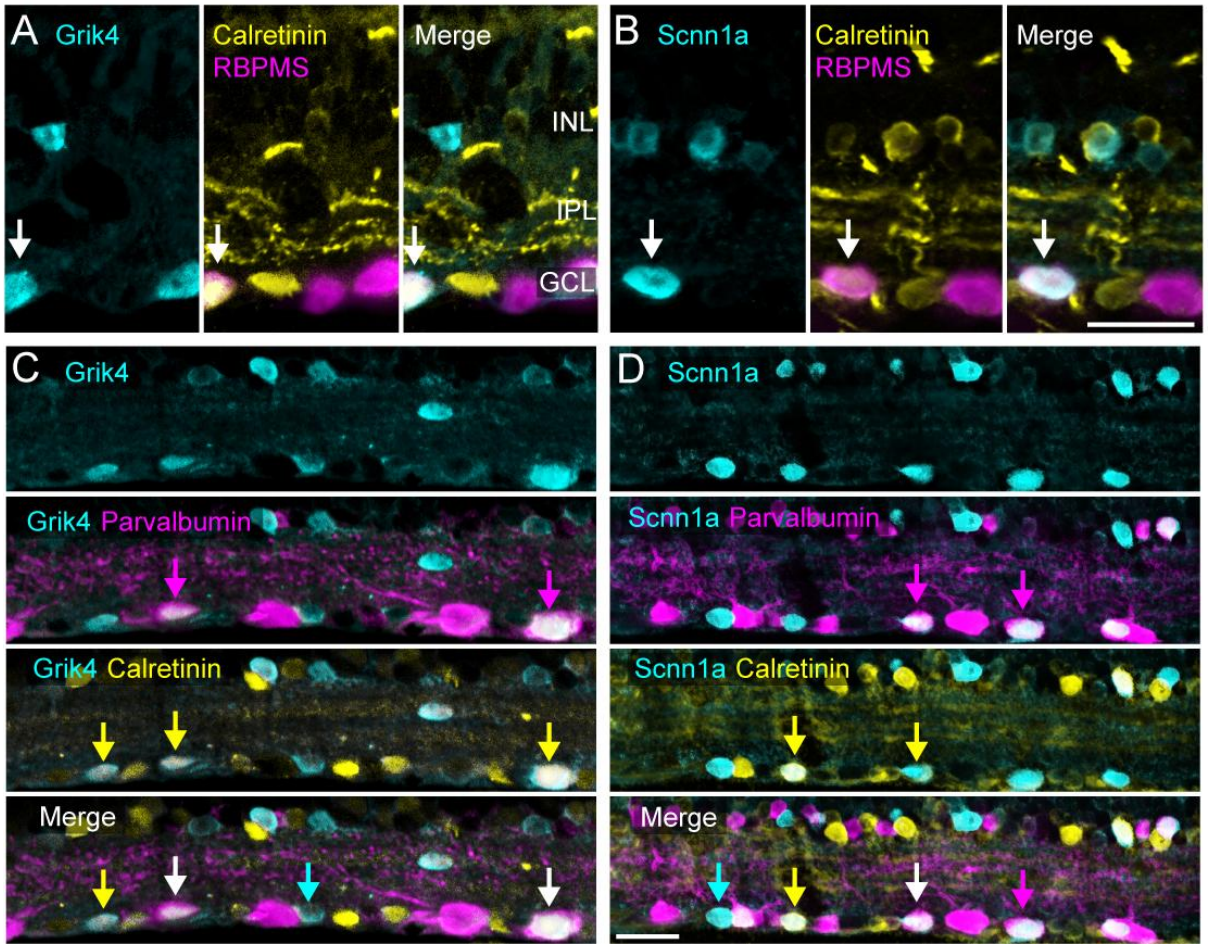

Figure 3: Grik4 and Scnn1a DREADD are expressed in multiple RGC types. Vertical sections of Grik4 and Scnn1a retinas were triple stained A, B) for GFP (cyan), RBPMS (magenta) and Calretinin (yellow) or C, D) GFP (cyan), Parvalbumin (magenta) and Calretinin (yellow). INL = inner nuclear layer, IPL = inner plexiform layer, GCL = ganglion cell layer. Scale bar in D = 20 µm.

of Grik4 and Scnn1a RGCs that were GFP/RBPMS/Calretinin positive (Fig A, B arrows) and GFP/RBPMS positive cells, which clearly demonstrates that there are at least two RGC types for each pool. We did not find any Calretinin positive Grik4 ACs, but we did find some Calretinin positive Scnn1a ACs. For technical reasons we were not able to combine RBPMS and Parvalbumin staining (both antibodies were raised in the same species). To extend on these findings and to further investigate if the genetic pools of Grik4 and Scnn1a consist of more than two RGC types, we triple-labelled vertical sections (Fig 3 C, D) for GFP (cyan), Calretinin (yellow) and Parvalbumin (magenta). Our initial findings indicate that the majority of GFP cells in the GCL are RGCs, thus these experiments aimed to estimate if these GFP cells can be subdivided into smaller groups. We found that the population of Grik4 (Fig 3 C) expressing cells (cyan) in the GCL consists of at least three different types of cells: only GFP (Fig 3 C, cyan arrow), GFP/Calretinin (yellow arrow) and GFP/Calretinin/Parvalbumin (white arrows) cells. It is likely that these three different cell types reflect RGCs and not dACs because we did not find any putative Grik4 ACs in the INL expressing Calretinin and/or Parvalbumin.

For the pool of Scnn1a expressing cells in the GCL (Fig 3 D), we found four different types: those expressing only GFP (Fig 3 D, cyan arrow), GFP/Calretinin (yellow arrow), GFP/Parvalbumin (magenta arrow) and GFP/Calretinin/Parvalbumin (white arrow) cells. A fraction of the GFP positive ACs in the INL were positive for Calretinin, suggesting that some GFP/Calretinin and GFP/Calretinin/Parvalbumin cells in the GCL are potentially dACs. In summary, the pool of Grik4 and Scnn1a cells in the GCL respectively consists of at least three and four different RGC types. That information is important for the validation of our novel approach to the functional classification of Grik4 and Scnn1a RGCs.

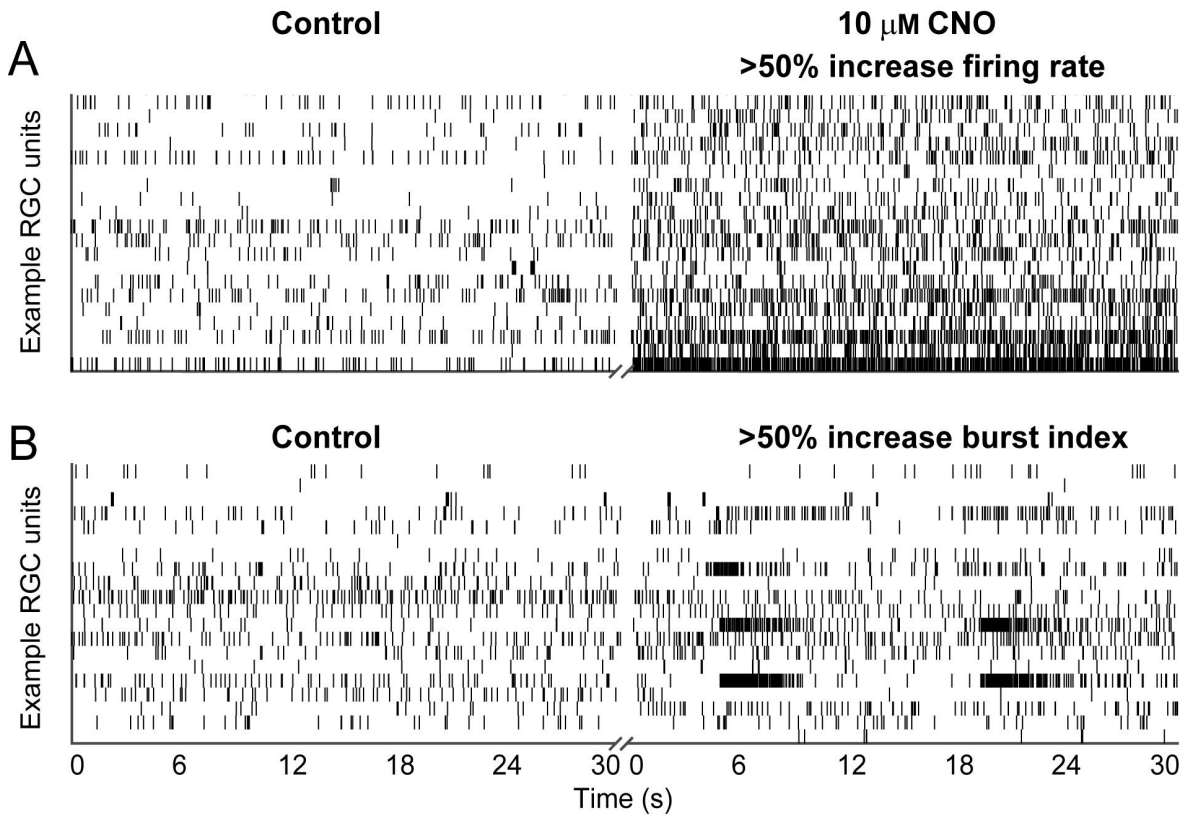

Figure 4: DREADD activation leads to spike pattern changes in retinal ganglion cells. DREADDs in retinal ganglion cells can be activated with Clozapine N-oxide (CNO) and lead to an increase of spiking (A, right half) and also increased bursting (B, right half). 20 control (without CNO) and CNO recordings of Grik4 retinal ganglion cells that showed a minimum of 50% change of activity in their spiking rate or burst were used as a representative example for the spike raster plot. Vertical lines represent spike times as plotted as a function of time.

We next identified Grik4 and Scnn1a RGCs according to the change of their spiking pattern following DREADD activation with CNO, and we grouped them into functional clusters based on response similarity. The IHC experiments revealed that DREADDs are expressed in several RGC types but also in ACs (albeit more sparsely). Hence, the first step to isolate Grik4 and Scnn1a expressing RGCs is to pre-identify cells that showed either a 50% (arbitrarily chosen) increase in spontaneous firing rate (Fig 4 A) or a 50% increase of the Burst Index (Fig 4 B) in the presence of CNO. That step is followed by correlating the physical position of these identified RGCs with microscope images of DREADD-GFP expressing cells in the GCL. This process allowed us to unequivocally correlate anatomical and functional features of Grik4 and Scnn1a RGCs.

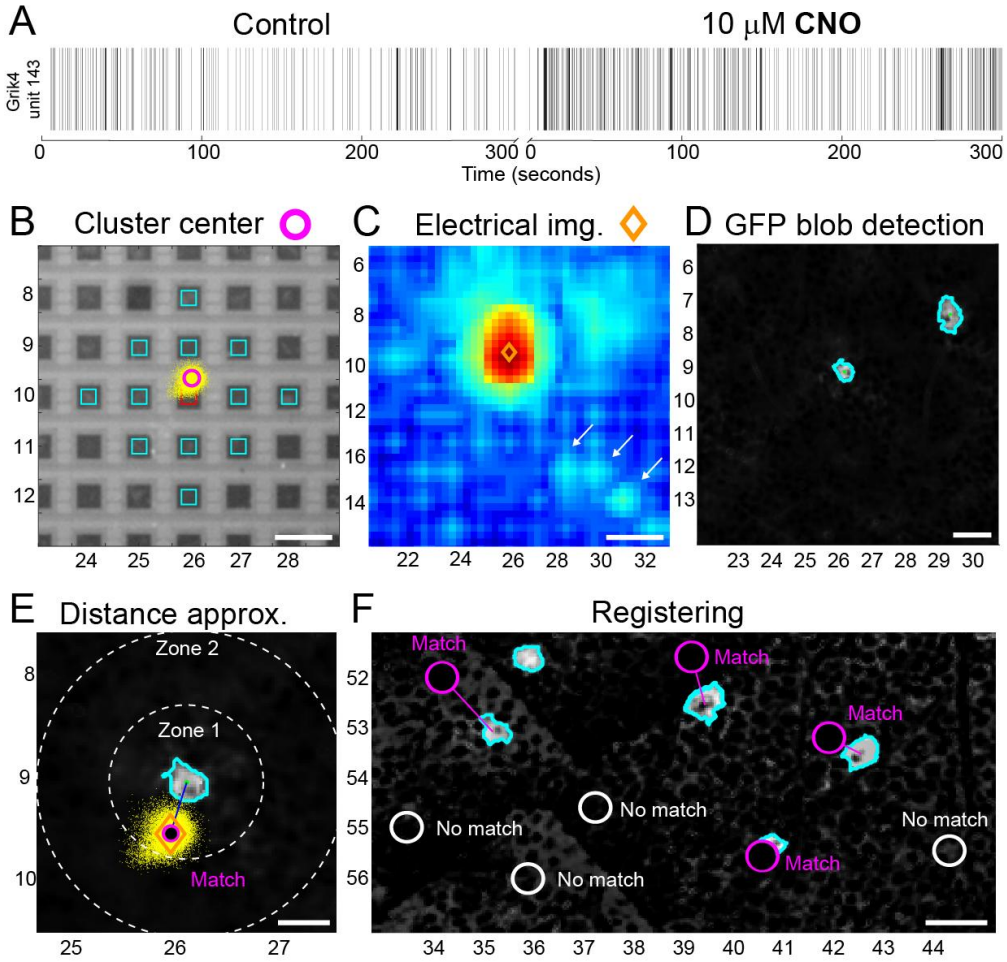

Figure 5: Registering GFP RGCs with nearby isolated spike center clusters. The spike cluster center (B, circle) and the electrical imaging (C, diamond) define the potential electrical source location of the isolated RGCs. Spike centers in close proximity to GFP labelled RGCs (D) were registered as potential DREADD-expressing RGCs (E, F, Match). Scale bars A, C, F = 40 µm; B = 80 µm; E = 20 µm.

In the next step, we provide a brief exemplary description, using an identified Grik4 RGC (Fig 5), to show how we register GFP labelled cells with their spiking activity for unambiguous identification of Grik4 and Scnn1a RGCs. Further technical details are available in the Method section. The spike localization cluster center (magenta circle) is calculated for a pre-identified (see above) Grik4 RGC (Fig 5 B) using the spike interpolation algorithm in Herdingspikes2. In addition, electrical imaging confirmed the maximal current sink position (Fig 5 C, orange diamond) and visualized putative axonal trajectories (Fig 5 C, arrows), thus helping to align the GFP cell structure with the electrical activity more precisely. Image segmentation techniques are used to threshold the GFP foreground from the background and a blob detection is applied to detect the outlines and center of Grik4 and Scnn1a GFP positive cells in the GCL (Fig 5 D, green outline). Lastly, the x and y position are converted to match with MEA images dimensions (Fig 5 E). Spikes originate from the axon initial segment (AIS) rather than from the cell body. Therefore, we expect the spike

cluster center to be slightly eccentric with respect to the soma itself. The exact location of the AIS in RGCs can be very close to the soma, or sometimes rather distant along the axon [33,34]. All the information from panels B-D is needed to estimate if a GFP-expressing cell corresponds to a nearby spike cluster center. Two virtual circles with a radius of 30 and 60 µM (arbitrary values) are drawn around a detected GFP blob center (Fig 5 E) and spike

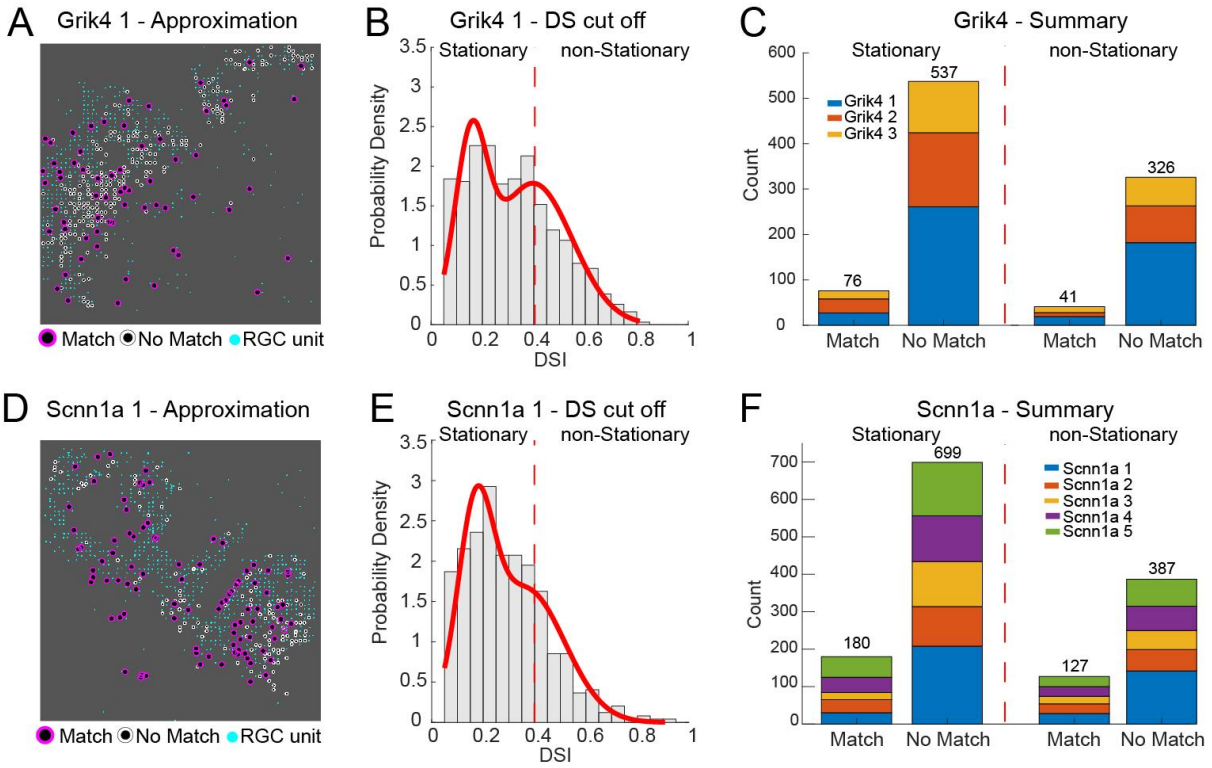

Figure 6: Dividing registered Grik4 and Scnn1a RGCs into stationary and non-stationary responders. Moving stimuli were used to estimate the direction selectivity index (DSI) of registered "Match" RGCs (Grik4 A, Scnn1a D, magenta). The DSI was plotted against the probability density (histogram) and fitted with two gaussians (B, E, red line). RGCs exceeding a set threshold (B, E, dotted red line) were labelled "non-Stationary". The registered RGCs from all retinas were grouped into "non-Stationary" and "stationary" and counted (C, F).

cluster centers falling within one of these two zones are registered. From experience, we reached the conclusion that using the 60 mm zone was sufficient to reliably determine whether an isolated spike cluster corresponds to a specific GFP-expressing cell. Such cases are referred to as "Match", and those falling outside these boundaries are classified as "No Match" (Fig 5 F, Fig 6 A, D). All other recorded spike units, that did not exhibit changes in spike behavior in the presence of CNO, were labelled "RGC unit" (Fig 6 A, D) but not further considered for classification.

We successfully analyzed 3 Grik4 and 5 Scnn1a retinas to register "Match" (Fig 6 A, D, magenta) and "No Match (Fig 6 A, D, white) cells. Figure 6 A, D are representative examples from the cohort of all experiments. Note that the recording area is generally not completely covering the entire 64 x 64 array. In total, we identified 117 "Match" and 863 "No Match"

RGC in the 3 Grik4 retinas (Fig 6 C) and 307 “Match” and 1066 “No Match” in the 5 Scnn1a retinas (Fig 6 F). We divided these RGCs according to their response preference for stationary (static, full field) and non-stationary (moving, orientations) images. Briefly, cells that were exceeding a threshold value (see Methods) for their direction or orientation selectivity index (DSI and OSI, respectively) were classified as non-stationary (Fig 6 B, E). Figure 6 is showing an example for DSI grouping but we also grouped cells according to their OSI. In the following, we focus on “Match” Grik4 and Scnn1a RGCs only. A total of 78 Grik4 stationary and 41 non-stationary RGCs were collected (Fig 6 C). For Scnn1a, 180 stationary and 127 non-stationary RGCs were collected (Fig 6 F). However, most RGCs did exhibit changes in firing rate (increase or decrease) without revealing any GFP signals, hence they are unlikely to be Grik4 or Scnn1a RGCs (here called “No Match”). These cells are most likely other RGC types affected by either Grik4 or Scnn1a expressing ACs, and they outnumber the “Match” RGCs. In summary, we successfully combined near pan-retinal recordings with *post hoc* anatomical characterization and isolated GFP-positive Grik4 and Scnn1a RGCs with increased spiking or bursting activity in the presence of CNO.

After the successful registration of spikes with Grik4/Scnn1a GFP RGCs, the final step is to classify these cells into functional groups according to the nature of their responses to light. We recently described a non-parametric approach for RGC classification by using the SPIKE distance [35,36] as a clustering metric [12]. In order to use that approach, it is necessary to have a stimulus that elicits responses simultaneously over the entire recording area. Here we used a chirp stimulus inspired from Baden et al (2016) [6] that elicits responses from all RGCs at the same timeto pre-sort stationary and non-stationary RGCs (chirp, Fig 7 B, F, top) for SPIKE distance measure and hierarchical agglomerative clustering. We manually validated our detected clusters by grouping several response parameters, e.g. bias index (ON, ON-OFF or OFF) or response duration (transient or sustained), from the chirp and moving bars (for example Fig 7 C-E, G). Manual grouping was only feasible because the expected cluster numbers for Grik4 and Scnn1a were small (respectively 3 and 4 according to our IHC analyses). The pairwise SPIKE distances were determined from all trials of the chirp stimulus and the resulting distance matrix of stationary and non-stationary RGCs was clustered with a hierarchical clustering algorithm followed by the construction of a dendrogram as shown in Jouty et al., 2018[12]. To find the optimal number of clusters for stationary and non-stationary SPIKE distances we used gap statistics [12,37]. For stationary and non-stationary RGCs, gap statistics estimated four response clusters of Grik4 RGCs (Fig 7 A). Additional response parameters were extracted from the chirp peri-stimulus time histogram (PSTH) e.g., bias index or response duration of these 4 stationary RGC types. We

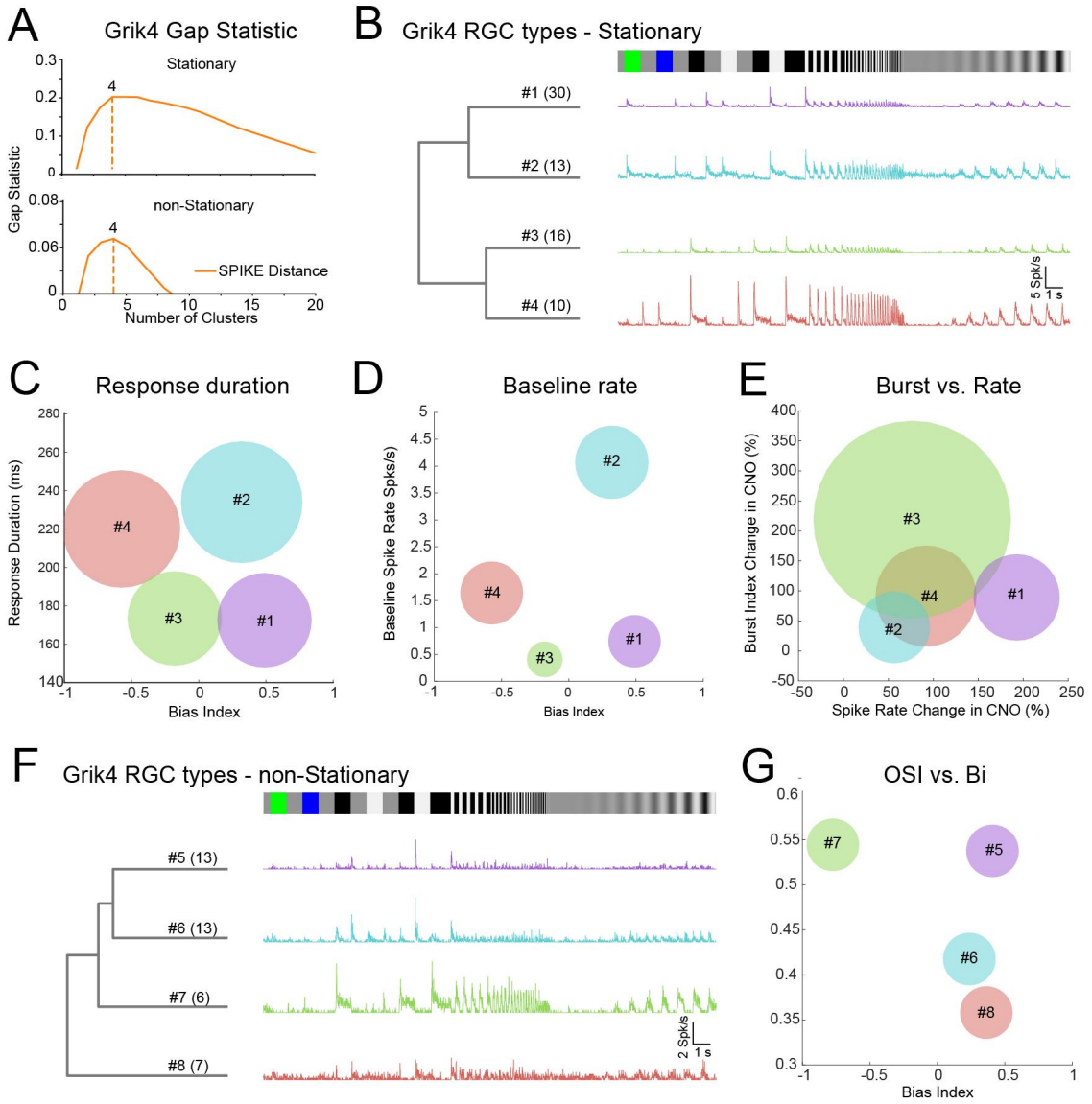

Figure 7: Clustering of Grik4 stationary and non-stationary RGC responses. RGC responses that showed a high spike train similarity for a chirp stimulus (B, F) were grouped together using gap statistics (A). For each RGC of the groups, the PSTH was calculated and the mean PSTH was plotted (B, F, colored lines). The means for Bias Index (C, D, G), Response Duration (C), Baseline Spiking (D), Burst change (E), Spike Rate change (E) and orientation selectivity index (OSI, G) index were scatter plotted and the standard deviation were used as the circle size.

found potentially ON transient (#1, n = 30), ON sustained (#2, n = 13), ON-OFF (#3, n = 16) and OFF sustained (#4, n = 10) response types. Some RGC units were discarded during the process of SPIKE distance grouping as they showed a low signal-to-noise ratio i.e., high response variability [12]. To validate these four detected clusters, we plotted the mean bias index against the mean response duration from all RGCs in a cluster (Fig 7 C), revealing four distinct groups that corresponded to the confirmed stationary RGC types. Moreover, spontaneous activity follows very specific patterns for certain types and can be used for RGC classification. Plotting the mean Bias Index against mean spontaneous firing rate (baseline firing) revealed that the ON sustained cluster #2 (Fig 7 B, C, cluster 2) exhibited a

very strong baseline firing rate (Fig 7 D). The same plot also shows that the three other RGC types have a moderate baseline firing rate and further confirmed the 4 well separated RGC types. Whether the spontaneous firing rate becomes burstier or simply increases monotonously in the presence of CNO can be used to further group RGCs into clusters (Fig 7 E). Interestingly, the effect of CNO on cluster #2 is minimal (Fig 7 E) whereas it is maximal for cluster #3 (Fig 7 E).

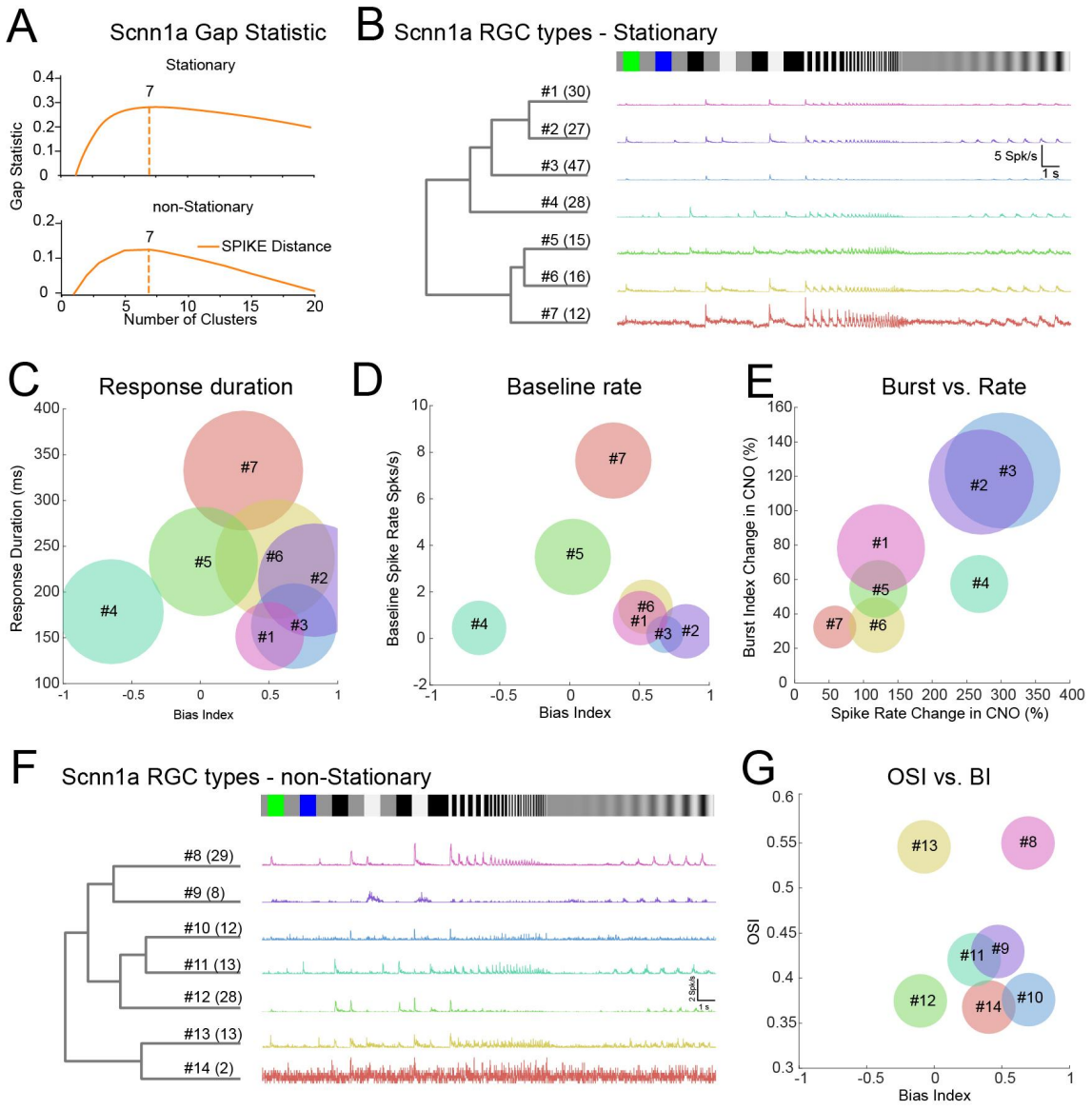

Figure 8: Clustering of Scnn1a stationary and non-stationary RGC responses. RGC responses that showed a high spike train similarity for a chirp stimulus (B, F) were grouped together using gap statistics (A). For each RGC of the groups, the PSTH was calculated and the mean PSTH was plotted (B, F, colored lines). The means for Bias Index (C, D, G), Response Duration (C), Baseline Spiking (D), Burst change (E), Spike Rate change (E) and orientation selectivity index (OSI, G) index were scatter plotted and the standard deviation were used as the circle size.

The non-stationary RGCs barely responded to the chirp stimulus (Fig 7 F, scale bar) but that response was, albeit modest, reliable and unique for the different clusters. We used the orientation (OS) and direction selectivity (DS) index in addition to the chirp PSTH parameters to define the four non-stationary Grik4 clusters (Fig 7 F, G). We found ON - OS (#5, n = 13), ON-OFF - DS (#6, n = 13; #8, n = 7) and OFF – OS (#7, n = 6) response groups in the pool of non-stationary Grik4 RGCs. The mean DS index was almost identical for these 4 groups, hence we used the OS index for manual validation. While the ON – OS (#5) and the OFF – OS (#7) are clearly distinguishable from each other, the difference is less pronounced between the two ON-OFF – DS clusters (#6 & #8). They have a similar mean BI, but Cluster 6 tends to be marginally more OS (Fig 7 G). Clusters 6 and 8 would therefore need further evaluation to determine whether they are truly different RGC types. In summary, we found 4 stationary RGCs types and most likely 3, non-stationary RGC types that share the Grik4 gene pool.

We proceeded in a similar way with stationary and non-stationary registered Scnn1a RGCs (Fig 8). Gap statistics suggested 7 clusters for both groups (Fig 8 A). The dendrogram of the chirp PSTH consists of ON transient (#1, n = 30; #2, n = 27; #3, n = 47), ON sustained (#6, n = 16; #7, n = 12), ON-OFF (#5, n = 15) and OFF (#4, n = 28) like response for Scnn1a RGC types (Fig 8 B). Further analysis revealed that the ON sustained (#7), OFF (#4) and ON-OFF (#5) response parameters (Fig 8 C - Bias Index vs Response Duration; Fig 8 D – Bias Index vs Baseline) were clearly distinct from each other. At the same time, the distinction is less clear between clusters #1, #2, #3, #6 (Fig 8 C, D). The effect of CNO on the different Scnn1a RGCs was also diverse (Fig 8 E) with #7 barely affected and #2 & #3 massively affected. The non-stationary Scnn1a RGCs (Fig 8 F) clustered into OFF-DS (#11, n = 13), ON-OFF– DS (#12, n = 28; #14, n = 2), ON-OFF – OS (#13, n = 13), ON – DS (#9, n = 8; #10, n = 12) and ON - OS (#8, n = 29) like responses. Although there was some overlap between certain clusters (#9, #10, #11, #14) when plotting the Bias Index and OS index means (Fig 8 G), their chirp PSTH plots were substantially different, suggesting that these cells do belong to distinct functional groups. Therefore it is likely that the Scnn1a RGC pool consists of several DS and OS cells which will necessitate further investigation to establish their basic functional differences. In summary, we found a minimum of four stationary and a maximum of seven non-stationary Scnn1a RGC types.

Discussion

We established a novel approach for RGC classification, based on grouping of cells sharing gene expression and similarities in their light response patterns. We successfully used excitatory DREADD activation in retinal cells in combination with immunohistochemistry and large-scale retinal electrophysiology to provide a pan-retinal phenotypical description of Grik4- and Scnn1a-expressing RGCs in the mouse retina. We extended the pre-existing list of Grik4 expressing RGC types and, for the first time, we provide a functional description of Scnn1a-expressing RGCs. We also showed that certain types of ACs express Grik4 and Scnn1a and that exciting these cells with DREADDs activation leads to spike firing change many undefined RGCs.

Our classification approach found 4 stationary and 4 non-stationary Grik4 RGC response clusters (see also supplemental table 1). Grik4 expression in the retina has been described [4,21–24] but there is functional characterization only for two RGC types [22,24]. These two known classes do match two of our own response clusters, which validates the usefulness of our approach. Johnson et al. (2018) [24] reported that the Grik4-expressing PixON RGC type is an ON sustained type and has strong spontaneous activity. Our Grik4 cluster #2 from the stationary RGCs has the same key phenotypic features - sustained responses and strong spontaneous activity. Hence it is likely that this cluster represents the PixON RGC type. Cluster #2 also matches with the ON sustained clusters 31/32 from Baden et al. (2016) [6]. Grik4 clusters #1, #3 and #4 potentially resemble clusters 29 (ON high freq), 15/16 (ON-OFF local) and 6 (OFF alpha sustained) from that study. The latter one is parvalbumin positive [6,15] and in line with our iIHC results that revealed Grik4 and parvalbumin expressing RGCs. Baden et al. (2016) found many more parvalbumin-expressing RGC types rather than the traditionally known 8 types [32]. We suspect that there is some overlap between Grik4 and yet undescribed parvalbumin, potentially also calretinin, RGC types. We currently investigate the functional features of parvalbumin and calretinin co-expressing RGCs using a similar methodology [38]. Further, the existence of Grik4-expressing ON-OFF – DS RGCs has been demonstrated in the mouse retina [22]. Cluster #6 of our non-stationary RGCs also show ON-OFF DS RGCs and potentially resemble clusters 17/18 (ON-OFF DS1) from Baden et al. (2016). Grik4 cluster #8 is also ON-OFF DS though the responses are less pronounced than in cluster #6. Our non-stationary Grik4 cluster #5 has similarities with cluster 24 (ON local trans - OS) and cluster #7 with cluster 1 (OFF local OS) from Baden et al. (2016). The latter one also shows similarities to the F-midi OFF cell responses described in Roussou et al. (2016)[39]. It would also explain the findings of parvalbumin and calretinin positive Grik4 RGCs in our experiments (Fig 3 C) since F-midi OFF cells are supposed to express both[39].

For Scnn1a, we found 7 stationary and 7 non-stationary RGC response groups (see also supplemental table 1). Interestingly, the Scnn1a ON sustained Cluster #7 showed remarkable similarity with the PixON characteristics described earlier - sustained responses and high baseline firing. There are no reports about Grik4 and Scnn1a co expressing cells but it is not uncommon that certain RGC types share the same genes e.g. *Foxp* and *Brn3[39]* or *Pvalb* and *Calb2[38–40]*. Our Scnn1a stationary clusters #1, #2, #3 and #6 were grouped by gap statistics into 4 different groups but our post-hoc analysis (Fig 8 C, D) suggests one group. Therefore, these four clusters may reflect just one, or maybe two functional groups. They all exhibit ON transient responses but are not able to follow high frequencies in the chirp (like cluster #1 in Grik4), thus they resemble clusters 26/27 (ON trans) in Baden et al. (2016). Cluster #4 has OFF transient response characteristics and could resemble 11/12 OFF alpha trans after Baden et al., 2016. The Scnn1a stationary cluster #5 shows weak ON and OFF responses to chirp and could potentially be the W3 local edge detector (cluster 14 in Baden et al. 2016). The grouping of the non-stationary Scnn1a clusters #8 - #14 shows a variety of response types. Scnn1a cluster #8 shows strong ON transient and slightly OS responses and may relate to cluster 26 (ON trans) or cluster 25 (ON trans OS) in Baden et al. (2016). Scnn1a cluster #9 shows very weak and sluggish ON DS responses and is not really following the oscillating components in the chirp. It shows similarities to cluster 36 (ON DS sust 2) from Baden et al. (2016). Our Scnn1a OFF DS cluster #11 is most likely cluster 2 (OFF DS) in Baden et al. (2016) and/or potentially the F-mini OFF described in Roussou et al. (2016). The F-mini OFF is calretinin (occasionally

parvalbumin as well) positive which would fit with our IHC results. The non-stationary Scnn1a ON-OFF DS cluster #12 may relate to clusters 17/18 (ON-OFF DS 1) while cluster #13, to cluster 20 (ON-OFF local OS) from Baden et al. 2016. Clusters #10 and #14 show very weak chirp responses and it is not feasible to assign them to any existing response type. In summary, our approach is able to group individually MEA recorded RGC response types into established response clusters (Baden et al. (2016)) obtained with Ca^{2+} imaging. However, we try to avoid a definite grouping and rather suggest some naming here for convenience. Further studies with co-staining of different RGC markers and/or transcription factors could provide more detailed response groups that share the same gene expression. Our approach has been scaled up with multiple labelling methods but it also increased the complexity and success rate [38]. Finding DREADD expression in ACs was initially challenging. We managed to circumvent the interference of DREADD activated ACs by combining MEA recordings with iIHC, which is not a straightforward solution and renders experiments much more complex. Our experimental design was based on Cre-Lox recombination, resulting in DREADD expression in all cells with the same promoter gene in the organism. In future work, DREADD expression should be targeted only to RGCs via viral transfection in order to avoid such strong side effects [41]. Blocking AC input onto postsynaptic targets (bipolar cells or RGCs) would be another solution, but has a big caveat: such disinhibition leads to massive increase in activity levels in all RGCs (Supp. Fig.1), hence masking RGC specific DREADD activation in specific subgroups where DREADDs are directly expressed on RGCs.

Our DREADD expression was not restricted to RGCs as initially designed. DREADDs were also expressed in one or several yet undescribed AC types. For Scnn1a, we found few GABAergic ACs but most GFP-positive ACs were not further characterized. For Grik4, we did not find any GABAergic ACs, nor were we able to define the AC type with our experimental means. Excitatory activation of Grik4 and Scnn1a ACs does have a profound effect on postsynaptic RGC activity. Indeed, most of our DREADD isolated RGCs (Figure 4) were not GFP positive (Figure 6). A single AC affects nearly every RGC within reach of its dendrites [42]. We did not investigate the nature of these RGCs affected by AC activity any further, nor did we investigate the underlying CNO affected circuits in the retina. Briefly, assuming that CNO acts simultaneously on some ACs and RGCs, we are confronted with the problem of untangling the underlying circuits. For example, let us consider a simple network with one population of DREADD ACs which modulate one population of bipolar cells and one population of DREADD) RGCs. Adding CNO will have a direct effect on RGCs, increasing their activity (firing rate or bursting rate). At the same time, ACs activity increases, thereby reinforcing lateral inhibition. This situation is already complex enough if we consider non linearities in the cell's responses But as those cells are embedded in a network, the net effect of CNO can have many forms leading to a priori undetermined situations. For example, it is known that cascade of inhibition can result in excitation (e.g. push-pull effect) [43]. A possible solution to this problem relies on a quantitative analysis requiring to consider the factors constraining individual cells responses, without and with CNO, and the network connectivity. As we checked, it is possible to propose in simple situations a map of CNO induced scenarios, in a suitable space of relevant biophysical parameters. These questions will be addressed on modelling and mathematical grounds in a forthcoming paper.

In summary, we have successfully isolated light-evoked responses in RGCs sharing gene expression by combining pharmacogenetics, large-scale retinal electrophysiology and

anatomy. We were able to extend the pre-existing list of Grik4 expressing RGC types and, for the first time, we provide a phenotypical description of Scnn1a-expressing RGCs. Our approach is not restricted to retinal cells but is widely applicable to other neurons from other brain regions. It is a scalable multimodal approach and can group large cohorts of neurons with similar gene expression very quickly. Here, we used only simplistic stimuli to design our RGC classification approach. We are currently investigating how these RGC groups contribute to the encoding of more complex visual scenes on a near pan-retinal scale. This data will shed light on how certain RGC types interact with each other across the retina, helping to develop a large-scale simulation platform, able to handle different visual processing circuits.

Methods

Animals and retina preparation

All experimental procedures were approved by the ethics committee at Newcastle University and carried out in accordance with the guidelines of the UK Home Office, under control of the Animals (Scientific Procedures) Act 1986. Grik4 (C57BL/6-Tg(Grik4-cre)G32-4Stl/J, the Jackson Laboratory, MA, JAX Stock No: 006474) and Scnn1a (B6;C3-Tg(Scnn1a-cre)3Aibs/J, JAX Stock No: 009613) mice were cross-bred with Gq-DREADD mice (B6N;129-Tg(CAG-CHRM3*,-mCitrine)1Ute/J, JAX Stock No: 026220) to generate a strain of mice with the excitatory Gq-DREADD expressed in Grik4 and Scnn1a expressing cells (from here on named: Grik4-DREADD and Scnn1a-DREADD, respectively). In addition, we crossbred the Grik4 and Scnn1a lines with an inhibitory DREADD (add info from Jax) but the effect on RGC firing rate was negligible and the litters were used only for immunofluorescence studies. Male and female wild-type, Grik4-DREADD and Scnn1a-DREADD mice, housed under a 12-hour light-dark cycle and aged between postnatal days (P) 53-148 were used for the experiments. Mice were dark-adapted overnight and killed by cervical dislocation. Eyes were enucleated, and following removal of the cornea, lens, and vitreous body, they were placed in artificial cerebrospinal fluid (aCSF) containing the following (in mM): 118 NaCl, 25 $NaHCO_3$, 1 NaH_2PO_4, 3 KCl, 1 $MgCl_2$, 2 $CaCl_2$, 10 glucose, and 0.5 l-Glutamine, equilibrated with 95% O_2 and 5% CO_2. The ventral and dorsal orientation was marked after enucleation. The retina was isolated from the eye cup and flattened for MEA recordings. For vertical cryosections, mouse eyecups were fixed in 4% paraformaldehyde (PFA; Alfa Aesar, MA) in 0.1 M phosphate buffer solution (PBS) for 2 x 20 minutes at room temperature and washed with PBS several times. For whole mounts, retinas were isolated from the eye cup and mounted on nitrocellulose paper (Sartorius, Germany) and transferred to 4% PFA in PBS (2 x 20 min), rinsed in PBS and prepared for further procedures. All procedures involving live animals and retinas were performed in dim red light and the room was maintained in darkness throughout the experiment.

Immunohistochemistry and image acquisition

After enucleation and fixation, the retinal tissue was processed in different ways for vertical and whole mount immunohistochemistry (IHC). For vertical sections, eyecups were cryoprotected in 30% sucrose in PBS overnight at 4°C and embedded in OCT Tissue TeK

(Sakura, NL) at -20°C on the following day. Vertical sections (15-20 µm) were cut on a OTF5000 cryostat (Bright Instruments, UK) and collected on Superfrost microscope slides (Thermo Fisher). Vertical sections and whole mounts were blocked with 10% normal goat serum (NGS) and/or 10% normal donkey serum (NDS) in PBS for at least 30 minutes at room temperature.

After the blocking procedure and a short rinse in PBS, Vertical sections were incubated with primary antibodies in 5% NGS (and/or NDS) + 1% Triton X-100 + PBS overnight at 4°C. Whole mounts were incubated free-floating with primary antibodies in 5% NGS (and/or NDS) + 1% Triton X-100 + PBS for 4-5 days at 4°C. Incubation with secondary antibodies in 1% Triton X-100 in PBS was carried out for 2 hours at room temperature for vertical sections or overnight at 4°C for whole mounts. Details of the primary antibodies are as follows: anti-GFP (chicken, Abcam 13970, 1:500-1000), anti-RBPMS (rabbit, Phosphosolutions 1830, 1:1000), anti-GABA (mouse, Sigma Aldrich A0310, 1:1000), anti-Calretinin (mouse, Swant 6B3, 1:1000) and anti-Parvalbumin (rabbit, Swant PV27, 1:1000). Secondary antibodies are as follows (all concentrations 1:500): goat anti-chicken CF488, goat anti-rabbit Alexa568/Alexa647 and donkey anti-mouse Alexa647. After washing several times with PBS, sections and whole mounts were mounted in Vectashield (Vector Laboratories, UK). All incubations and washing procedures were performed in the dark.

Images were captured using either a Zeiss Axio Imager upright microscope with Apotome structured illumination fluorescence (using 20x/40x air objectives) or a Zeiss LSM800 confocal microscope with 40x oil objective (Zeiss, Germany) operated with Zen software. Whole mount images were stitched together using Zen software, all other image postprocessing was done with Fiji (https://fiji.sc), Adobe Photoshop (Adobe, CA) and MATLAB (Mathworks, MA). The steps between single sections of confocal stacks were not exceeding 1 µm and 3 - 5 sections were superimposed with Fiji for presentation. For the cell density maps, cells were manually counted using the “Cell Counter” plugin in Fiji and a bivariate histogram (MATLAB *hist3*, bin size 60 x 60 µm) was calculated for the cell densities. For visualizing purposes, a 2-D Gaussian filtering was applied (MATLAB *imgaussfilt*, sigma 3).

Large-scale, high-density multielectrode array recordings and light stimulation

Recordings were performed on the BioCamX platform with high-density-multielectrode array (HD-MEA) Arena chips (3Brain GmbH, Lanquart, Switzerland), integrating 4096 square microelectrodes in a 2.67 x 2.67 mm area and aligned in a square grid with 42 mM spacing. The isolated retina was placed, RGC layer facing down, onto the MEA chip and flattened by placing a small piece of translucent polyester membrane filter (Sterlitech Corp., Kent, WA, USA) on the retina followed by a home-made anchor. Retinas were maintained at 33°C using an in-line heater (Warner Instruments LLC, Hamden, CT, USA) and continuously perfused using a peristaltic pump (~1 ml min−1). Retinas were left to settle on the MEA for at least 2 hours before recording. The platform records at a sampling rate of ~18 kHz/electrode when using the full 64×64 array. Recordings are filtered at 50Hz high-pass filter using BrainWaveX software (3Brain) and stored in hdf5-based data format. Spikes were detected and sorted using Herdingspikes2 (https://github.com/mhhennig/HS2) as in [19]. Briefly, spikes were first detected as threshold crossings individually on each channel, and then merged into unique events based on spatial and temporal proximity. For each detected

spike, a location was estimated based on the signal centre of mass. Spike sorting was performed by clustering all events using a feature vector consisting of the locations and the first two principal components of the largest waveform.

Light stimuli were projected onto the retina as described elsewhere [17]. Briefly, the projector irradiance was attenuated using neutral density filters to mesopic light levels (white 4 $\mu W/cm^2$). For stimuli we used a full field 'chirp' stimulus (see Fig 7, 8) consisting of various 1-sec contrast steps, increasing frequency (1-15Hz) and contrast modulations (1-93 Michelson contrast) which was repeated 5 times. We also used random black and white moving bars (width 100 mM, 12 directions (30° separation)), 800 mm/s, and the whole sequence repeated 5 times. For the chirp and motion stimuli, we estimated each unit's instantaneous firing rate for the different stimuli by convolving its spike train with a Gaussian kernel smoothing function (standard deviation (SD) = 25 ms). We then averaged the trials and extracted several features including the Bias Index and the response duration (see [19]). On average, recording from one retina yields light responses from hundreds to thousands of individual RGCs.

Registering RGC activity with IHC – blood vessels as reference marker

To register RGC activity with IHC, we used pre- and post-labelled blood vessels as reference markers. For pre-labelled blood vessel staining, the eye cup was incubated for 1 hr in aCSF + 5 µM Sulforhodamine 101 (SR101, Sigma Aldrich, MO) and afterwards transferred to aCSF + 0.06 µM SR101 for MEA recording procedures. After recording, the weight and the polyester membrane were carefully removed to expose the retina, and the MEA well rinsed with aCSF. If the blood vessels were not visible, a 50% Optiprep (Sigma Aldrich, MO) /50% aCSF solution was used for rinsing and further clearing. The MEA chip was mounted on a microscope stage (Olympus AX70, CoolLED pE fluorescence) while continuing rinsing every 2-3 min with oxygenated aCSF to ensure the tissue remains healthy throughout the procedure. The best stained blood vessel layer (either superficial or deep vascular plexus) was meander-like imaged. For every captured blood vessel image, images were acquired in the same location all the way down to the electrodes as well. Neighboring images were manually stitched together in Adobe Photoshop (Adobe, CA) later. The retina was then carefully removed from the MEA, flattened on a nitrocellulose membrane for IHC procedure. Blood vessel staining was enhanced by using an anti-mouse secondary antibody in the same excitation spectrum (normally Alexa568) and blood vessels were imaged again (same plexus as while the retina was imaged on the MEA). Both blood vessel staining images, pre- and post-tissue fixation were correlated with each other using the Control Point Selection Tool in Matlab. Briefly, the images taken in the live retina on the MEA were used as the fixed (reference) image and images acquired post fixation as the moving image. Minimum 50 reference points were picked for the fixed and moving images to create a geometric transformation (Matlab *fitgeotrans, lwm, 50*). That geometric transformation was applied to the GFP image. A stack (hereafter called MEA images) with the MEA electrode image, blood vessels pre- and post-fixation and GFP image was created in Adobe Photoshop.

Registering RGC activity with IHC – Grik4/Scnn1a DREADD RGC identification

The main procedure to identify and register RGC activity (spike clusters) with the MEA images is described in the main results (Figures 4, 5). Only units that did show a significant

change in spontaneous firing rate (sampled during at least 5 min) before and after adding CNO to the chamber were selected for Grik4/Scnn1a RGC identification and response clustering. Units with either >50% or <50% change in firing rate in CNO were considered as potential Grik4/Scnn1a candidates. We also used the Burst Index [44] to look at potential changes in activity levels induced by CNO, with potential Grik4/Scnn1a cells having changes in their Burst Index exceeding +/- 50%. Only these selected RGCs were further identified in the next steps.

During the spike sorting process with Herdingspikes2, the physical x and y spike localization for each detected spike from a single RGC unit is calculated (Figure 5 B). The spike location coordinates are given for a 64 x64 grid (the electrode layout of our MEA). Occasionally, we confirmed the cluster center (e.g., the center of mass of negative spike amplitude peaks) calculated by Herdingspikes2 by overlaying the x and y localization for the negative voltage peak (Figure 5 C magenta diamond) obtained through electrical imaging. For electrical imaging, the voltage fluctuations from the spike origin electrode and the neighboring 7 electrode rows and columns were read out. For a minimum of 1000 spikes per RGC unit, voltage fluctuations before and after (here 5 ms) each spike were normalized, and maximally projected with absolute values (Figure 5C) to visualize the current sink and the axonal trajectories. The spike localization and current sink coordinates were multiplied using a scaling factor to match the MEA images stack. GFP images were transformed to 8-bit images, a threshold (Matlab *max entropy*) was applied, potential gaps filled (Matlab *imfill 'holes'*) and binarized (Matlab *bwareaopen 50*). The binary image was analyzed (Matlab *regionprops*) and the centroids and diameters for every potential GFP blob was calculated. The pairwise distance between centroids and spike locations was calculated for all combinations.

Registering RGC activity with IHC – Grik4/Scnn1a response clustering

All potential Grik4/Scnn1a RGC units linked to a GFP blob (see Results) were further analyzed and grouped according to their response to a chirp stimulus. But before that grouping, cells were pre-classified into motion sensitive (responding preferably to either direction or orientation of motion) or cells that respond best to static stimuli (full field, chirp). We calculated the direction (DSI) and orientation (OSI) selectivity index as described elsewhere [19] but used a cut-off value for every experiment independently. Briefly, we fitted the tabulated data with a mixture of two gaussians (Figure 6 B, E). The fit parameters were computed using maximum likelihood parameter estimates (Matlab *mle*) and mu2 (the second peak, Figure 6 B, E) was used as cut-off value. The trail variability and signal to noise ratio was calculated [19] for each stationary/non-stationary RGC, and units with a value below the 25th percentile were discarded. The chirp responses of the remaining Grik4 and Scnn1a stationary/non-stationary RGC units were used to establish response groups. We used a similar approach to calculate the SPIKE distance as described in our earlier work [12]. Briefly, the SPIKE distances were computed using the open-source package PYSPIKE [36]. The pairwise distances between two units were determined by computing the pairwise distances of all trials of the chirp stimulus. The resulting distance matrix was then clustered with a hierarchical clustering algorithm (Python, *Scipy library dendrogram*). Matlab and Python scripts and other supplemental material will be made available via https://github.com/GerritHilgen/DREADD_RGCclass.

Acknowledgments

This project is funded by the Leverhulme Trust (RPG-2016-315 to ES and BC), by Newcastle University (Faculty of Medical Sciences Graduate School and Pro-Vice Chancellor Discretionary Fund) . We want to thank Matthias Hennig for help with the SPIKE distance calculations and Chris Williams who worked on other, unpublished aspects of the project. We also want to thank the Bioimaging Unit at Newcastle University for providing excellent service and help for this project.

Figure legends

Figure 1: Grik4 and Scnn1a cells in the GCL are not spatially homogeneous distributed. Whole mount antibody staining against Grik4 (A) and Scnn1a (B) DREADD GFP were imaged at the level of the ganglion cell layer. All stained GFP cells were counted and the densities per mm^2 were calculated and presented in pseudocolors for 3 Grik4 (C) and Scnn1a (D) retinas.V= ventral, T = temporal, D = dorsal, N = nasal. Scale bar A, B = 1 mm; Scale bar A, B insets II = 100 µm.

Figure 2: Grik 4 and Scnn1a DREADD are expressed in RGCs and ACs. Vertical sections were stained for Grik 4 (A, C, cyan) and Scnn1a (B, D, cyan) GFP. Sections were further co-labelled with RBPMS (A, B, magenta), a marker for retinal ganglion cells, and GABA (C, D, magenta). INL = inner nuclear layer, IPL = inner plexiform layer, GCL = ganglion cell layer. Scale bar in D = 20 µm.

Figure 3: Grik4 and Scnn1a DREADD are expressed in multiple RGC types. Vertical sections of Grik4 and Scnn1a retinas were triple stained A, B) for GFP (cyan), RBPMS (magenta) and Calretinin (yellow) or C, D) GFP (cyan), Parvalbumin (magenta) and Calretinin (yellow). INL = inner nuclear layer, IPL = inner plexiform layer, GCL = ganglion cell layer. Scale bar in D = 20 µm.

Figure 4: DREADD activation leads to spike pattern changes in retinal ganglion cells. DREADDs in retinal ganglion cells can be activated with Clozapine N-oxide (CNO) and lead to an increase of spiking (A, right half) and also increased bursting (B, right half). 20 control (without CNO) and CNO recordings of Grik4 retinal ganglion cells that showed a minimum of 50% change of activity in their spiking rate or burst were used as a representative example for the spike raster plot. Vertical lines represent spike times as plotted as a function of time.

Figure 5: Registering GFP RGCs with nearby isolated spike center clusters. The spike cluster center (B, circle) and the electrical imaging (C, diamond) define the potential electrical source location of the isolated RGCs. Spike centers in close proximity to GFP labelled RGCs (D) were registered as potential DREADD-expressing RGCs (E, F, Match). Scale bars A, C, F = 40 µm; B = 80 µm; E = 20 µm.

Figure 6: Dividing registered Grik4 and Scnn1a RGCs into stationary and non-stationary responders. Moving stimuli were used to estimate the direction selectivity index (DSI) of registered “Match” RGCs (Grik4 A, Scnn1a D, magenta). The DSI was plotted against the probability density (histogram) and fitted with two gaussians (B, E, red line). RGCs exceeding a set threshold (B, E, dotted red line) were labelled “non-Stationary”. The registered RGCs from all retinas were grouped into “non-Stationary” and “stationary” and counted (C, F).

Figure 7: Clustering of Grik4 stationary and non-stationary RGC responses. RGC responses that showed a high spike train similarity for a chirp stimulus (B, F) were grouped together using gap statistics (A). For each RGC of the groups, the PSTH was calculated and the mean PSTH was plotted (B, F, colored lines). The means for Bias Index (C, D, G), Response Duration (C), Baseline Spiking (D), Burst change (E), Spike Rate change (E) and orientation selectivity index (OSI, G) index were scatter plotted and the standard deviation were used as the circle size.

Figure 8: Clustering of Scnn1a stationary and non-stationary RGC responses. RGC responses that showed a high spike train similarity for a chirp stimulus (B, F) were grouped together using gap statistics (A). For each RGC of the groups, the PSTH was calculated and the mean PSTH was plotted (B, F, colored lines). The means for Bias Index (C, D, G), Response Duration (C), Baseline Spiking (D), Burst change (E), Spike Rate change (E) and orientation selectivity index (OSI, G) index were scatter plotted and the standard deviation were used as the circle size.

References

1. Euler T, Haverkamp S, Schubert T, Baden T. Retinal bipolar cells: elementary building blocks of vision. Nat Rev Neurosci. 2014;15: 507–519.

2. Curcio CA, Allen KA. Topography of ganglion cells in human retina. The Journal of Comparative Neurology. 1990. pp. 5–25. doi:10.1002/cne.903000103

3. Jeon C-J, Strettoi E, Masland RH. The Major Cell Populations of the Mouse Retina. The Journal of Neuroscience. 1998. pp. 8936–8946. doi:10.1523/jneurosci.18-21-08936.1998

4. Martersteck EM, Hirokawa KE, Evarts M, Bernard A, Duan X, Li Y, et al. Diverse Central Projection Patterns of Retinal Ganglion Cells. Cell Rep. 2017;18: 2058–2072.

5. Masland RH. The fundamental plan of the retina. Nat Neurosci. 2001;4: 877–886.

6. Baden T, Berens P, Franke K, Román Rosón M, Bethge M, Euler T. The functional diversity of retinal ganglion cells in the mouse. Nature. 2016;529: 345–350.

7. Grünert U, Martin PR. Cell types and cell circuits in human and non-human primate retina. Prog Retin Eye Res. 2020; 100844.

8. Reinhard K, Münch TA. Visual properties of human retinal ganglion cells. PLoS One.

2021;16: e0246952.

9. Coombs J, van der List D, Wang G-Y, Chalupa LM. Morphological properties of mouse retinal ganglion cells. Neuroscience. 2006;140: 123–136.

10. Völgyi B, Chheda S, Bloomfield SA. Tracer coupling patterns of the ganglion cell subtypes in the mouse retina. J Comp Neurol. 2009;512: 664–687.

11. Zeck GM, Masland RH. Spike train signatures of retinal ganglion cell types. Eur J Neurosci. 2007;26: 367–380.

12. Jouty J, Hilgen G, Sernagor E, Hennig MH. Non-parametric Physiological Classification of Retinal Ganglion Cells in the Mouse Retina. Front Cell Neurosci. 2018;12: 481.

13. Sanes JR, Masland RH. The types of retinal ganglion cells: current status and implications for neuronal classification. Annu Rev Neurosci. 2015;38: 221–246.

14. Rheaume BA, Jereen A, Bolisetty M, Sajid MS, Yang Y, Renna K, et al. Single cell transcriptome profiling of retinal ganglion cells identifies cellular subtypes. Nat Commun. 2018;9: 2759.

15. Laboissonniere LA, Goetz JJ, Martin GM, Bi R, Lund TJS, Ellson L, et al. Molecular signatures of retinal ganglion cells revealed through single cell profiling. Sci Rep. 2019;9: 15778.

16. Gollisch T, Meister M. Rapid neural coding in the retina with relative spike latencies. Science. 2008;319: 1108–1111.

17. Portelli G, Barrett JM, Hilgen G, Masquelier T, Maccione A, Di Marco S, et al. Rank Order Coding: a Retinal Information Decoding Strategy Revealed by Large-Scale Multielectrode Array Retinal Recordings. eNeuro. 2016;3. doi:10.1523/ENEURO.0134-15.2016

18. Marblestone* AH, Zamft* BM, Maguire YG, Shapiro MG, Cybulski TR, Glaser JI, et al. Physical principles for scalable neural recording. Front Comput Neurosci. 2013;7. doi:10.3389/fncom.2013.00137

19. Hilgen G, Pirmoradian S, Pamplona D, Kornprobst P, Cessac B, Hennig MH, et al. Pan-retinal characterisation of Light Responses from Ganglion Cells in the Developing Mouse Retina. Sci Rep. 2017;7: 42330.

20. Nakazawa K, Quirk MC, Chitwood RA, Watanabe M, Yeckel MF, Sun LD, et al. Requirement for hippocampal CA3 NMDA receptors in associative memory recall. Science. 2002;297: 211–218.

21. Ivanova E, Hwang G-S, Pan Z-H. Characterization of transgenic mouse lines expressing Cre recombinase in the retina. Neuroscience. 2010;165: 233–243.

22. Rivlin-Etzion M, Zhou K, Wei W, Elstrott J, Nguyen PL, Barres BA, et al. Transgenic mice reveal unexpected diversity of on-off direction-selective retinal ganglion cell subtypes and brain structures involved in motion processing. J Neurosci. 2011;31: 8760–8769.

23. Pisano F, Zampaglione E, McAlinden N, Roebber J, Dawson MD, Mathieson K, et al. Large scale matching of function to the genetic identity of retinal ganglion cells. Sci Rep. 2017;7: 15395.

24. Johnson KP, Zhao L, Kerschensteiner D. A Pixel-Encoder Retinal Ganglion Cell with Spatially Offset Excitatory and Inhibitory Receptive Fields. Cell Rep. 2018;22: 1462–1472.

25. Madisen L, Zwingman TA, Sunkin SM, Oh SW, Zariwala HA, Gu H, et al. A robust and high-throughput Cre reporting and characterization system for the whole mouse brain. Nat Neurosci. 2010;13: 133–140.

26. Armbruster BN, Li X, Pausch MH, Herlitze S, Roth BL. Evolving the lock to fit the key to create a family of G protein-coupled receptors potently activated by an inert ligand. Proc Natl Acad Sci U S A. 2007;104: 5163–5168.

27. Roth BL. DREADDs for Neuroscientists. Neuron. 2016;89: 683–694.

28. Urban DJ, Roth BL. DREADDs (designer receptors exclusively activated by designer drugs): chemogenetic tools with therapeutic utility. Annu Rev Pharmacol Toxicol. 2015;55: 399–417.

29. Zhu H, Aryal DK, Olsen RHJ, Urban DJ, Swearingen A, Forbes S, et al. Cre-dependent DREADD (Designer Receptors Exclusively Activated by Designer Drugs) mice. Genesis. 2016;54: 439–446.

30. Rodriguez AR, de Sevilla Müller LP, Brecha NC. The RNA binding protein RBPMS is a selective marker of ganglion cells in the mammalian retina. Journal of Comparative Neurology. 2014. pp. 1411–1443. doi:10.1002/cne.23521

31. Lee E-S, Lee J-Y, Jeon C-J. Types and density of calretinin-containing retinal ganglion cells in mouse. Neurosci Res. 2010;66: 141–150.

32. Yi C-W, Yu S-H, Lee E-S, Lee J-G, Jeon C-J. Types of parvalbumin-containing retinotectal ganglion cells in mouse. Acta Histochem Cytochem. 2012;45: 201–210.

33. Verbist C, Müller MG, Mansvelder HD, Legenstein R, Giugliano M. The location of the axon initial segment affects the bandwidth of spike initiation dynamics. PLoS Comput Biol. 2020;16: e1008087.

34. Colbert CM, Johnston D. Axonal action-potential initiation and Na+ channel densities in the soma and axon initial segment of subicular pyramidal neurons. J Neurosci. 1996;16: 6676–6686.

35. Kreuz T, Chicharro D, Houghton C, Andrzejak RG, Mormann F. Monitoring spike train synchrony. J Neurophysiol. 2013;109: 1457–1472.

36. PySpike—A Python library for analyzing spike train synchrony. SoftwareX. 2016;5: 183–189.

37. Tibshirani R, Walther G, Hastie T. Estimating the number of clusters in a data set via the gap statistic. J R Stat Soc Series B Stat Methodol. 2001;63: 411–423.

38. Hilgen G, Lockwood E, Ratcliff JEJ, Sernagor E. Pan-retinal characterization of parvalbumin-calretinin co-expressing cells in the mouse retina. F1000Res. 2019;8. doi:10.7490/f1000research.1117479.1

39. Rousso DL, Qiao M, Kagan RD, Yamagata M, Palmiter RD, Sanes JR. Two Pairs of ON and OFF Retinal Ganglion Cells Are Defined by Intersectional Patterns of Transcription Factor Expression. Cell Rep. 2016;15: 1930–1944.

40. Kovács-Öller T, Szarka G, Tengölics ÁJ, Ganczer A, Balogh B, Szabó-Meleg E, et al. Spatial Expression Pattern of the Major Ca-Buffer Proteins in Mouse Retinal Ganglion Cells. Cells. 2020;9. doi:10.3390/cells9040792

41. Storchi R, Milosavljevic N, Eleftheriou CG, Martial FP, Orlowska-Feuer P, Bedford RA, et al. Melanopsin-driven increases in maintained activity enhance thalamic visual response reliability across a simulated dawn. Proc Natl Acad Sci U S A. 2015;112: E5734–43.

42. de Vries SEJ, Baccus SA, Meister M. The projective field of a retinal amacrine cell. J Neurosci. 2011;31: 8595–8604.

43. Deny S, Ferrari U, Macé E, Yger P, Caplette R, Picaud S, et al. Multiplexed computations in retinal ganglion cells of a single type. Nat Commun. 2017;8: 1964.

44. Jones TA, Leake PA, Snyder RL, Stakhovskaya O, Bonham B. Spontaneous discharge patterns in cochlear spiral ganglion cells before the onset of hearing in cats. J Neurophysiol. 2007;98: 1898–1908.

Supplement

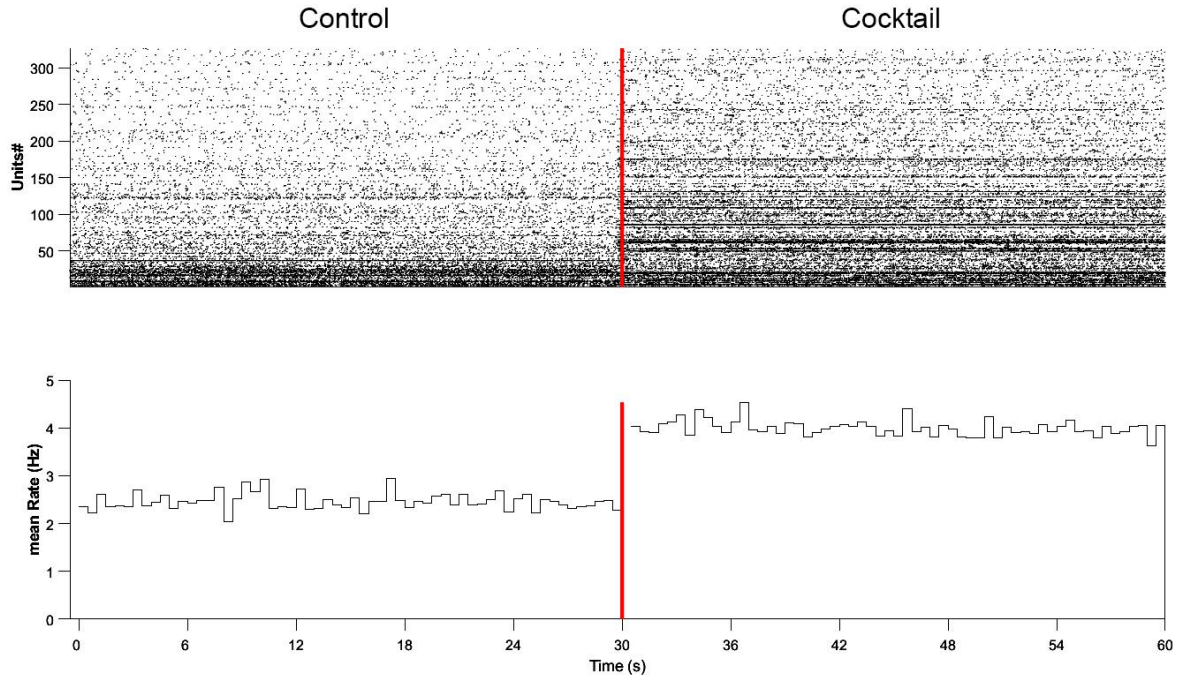

Supplemental Figure 1: Spike activity in control and in the presence of an “allround" AC neurotransmitter blocker (*Cocktail*) from randomly selected Scnn1a RGC units (Scnn1a experiment no 4, see Fig 6). The cocktail contains: 2 µM Strychnine (glycine receptor antagonist), 20 µM Mecamylamine (nicotinic acetylcholine receptor antagonist), 20 µM Bicuculline ($GABA_A$ antagonist), 5 µM CGP 55845 ((2*S*)-3-[[(1*S*)-1-(3,4-Dichlorophenyl)ethyl]

amino-2-hydroxypropyl](phenylmethyl)phosphinic acid hydrochloride, $GABA_B$ antagonist), 50 µM TPMPA (1,2,5,6-Tetrahydropyridin-4-yl methylphosphinic acid, $GABA_C$ antagonist).

	Grik 4 stationary	**Scnn1a stationary**	**Grik4 non-stationary**	**Scnn1a non-stationary**
Cluster here	Cluster after Baden et al. 2016			
#1	29 ON high freq	26/27 ON trans		
#2	31/32 ON sustained (PixON)	26/27 ON trans		
#3	15/16 ON-OFF local	26/27 ON trans		
#4	6 OFF alpha sustained	11/12 OFF alpha trans		
#5		14 W3 local edge detector	24 ON local trans OS	
#6		26/27 ON trans	17/18 ON-OFF DS1	
#7		31/32 ON sustained (PixON)	1 OFF local OS (F-midi OFF)	
#8			17/18 ON-OFF DS1 (less pronounced)	25/26 ON trans (OS)
#9				36 ON DS sustained 2
#10				?
#11				2 OFF DS (F-mini OFF)
#12				17/18 ON-OFF DS1
#13				20 ON-OFF local OS
#14				?

Supplemental table 1: Summary of found clusters and potential matches with Baden et al., 2016. NB these are suggestions.